Measurement of optical functions of highly oriented pyrolytic graphite in the visible

G. E. Jellison, Jr., J. D. Hunn, and Ho Nyung Lee
Materials Science and Technology Division, Oak Ridge National Laboratory, Oak Ridge, Tennessee 37831-6030, USA
(Received 9 May 2007; published 24 August 2007)

The spectroscopic dielectric functions of highly oriented pyrolytic graphite (HOPG) are determined at nine different wavelengths from 405 to 750 nm (3.06–1.65 eV). This determination is made on the basis of two ellipsometry measurements: (1) Standard ellipsometry measurements are performed on HOPG with the *c* axis perpendicular to the sample surface, and (2) two-modulator generalized ellipsometry microscope (2-MGEM) measurements are performed on HOPG cut and polished such that the *c* axis is parallel to the sample surface. Both the ordinary and extraordinary complex dielectric functions show nonzero absorption throughout the observed spectral range, while the ordinary dielectric function shows Drude-like behavior at longer wavelengths. From this, it can be concluded that graphite is metallic for visible light polarized parallel to the graphene planes, but acts more as a semiconductor or semimetal for visible light polarized perpendicular to the graphene planes. The 2-MGEM technique can also be used to generate images of the diattenuation, retardation, and direction of the principal axis.

DOI: 10.1103/PhysRevB.76.085125 PACS number(s): 78.20.Ci, 78.30.Er, 42.25.Ja

I. INTRODUCTION

Solid state carbon exists in many forms, including diamond, graphite, amorphous carbon, carbon nanotubes, and fullerenes (bucky balls).[1] This variety is due to the ability of carbon atoms to form linear, trigonal, or tetrahedral bonds (hybridized as sp, sp^2, and sp^3); in pure carbon materials, the bonding is primarily sp^2 or sp^3. The manifestations of the different bonding configurations on physical properties are extensive. Diamond (carbon in its pure sp^3 state) is one of the hardest materials known and is an electrical insulator with a band gap >5 eV, while graphite (in its nearly pure sp^2 crystalline state) is soft and metallic for conduction in the *a-b* plane. Amorphous carbon is a mixture of sp^2 and sp^3 hybridized carbon atoms, which results in metallic or semiconducting material, depending on the hybridization ratio and several other factors.

Apart from the diamond form, it has been very difficult to obtain accurate measurements of the optical functions (such as the refractive index and extinction coefficient) for any of these forms of carbon. This is particularly true for graphite, in spite of its obvious importance for applications. The primary reason for this lack of good data is that large single crystals of graphite do not exist. The closest material to single crystal graphite is highly oriented pyrolytic graphite (HOPG), which is made by the pyrolysis of carbonaceous vapor at 2000 °C followed by a ~3000 °C anneal.[2]

X-ray crystallography[3] of HOPG shows that graphite crystallizes in a hexagonal structure with the carbon atoms forming six-membered rings and the hybridization being nearly pure sp^2. Graphite may crystallize in a flat structure (space group: $P6_3/mmc$, point group: D_{6h} or $6/mmm$) or a buckled structure (space group: $P6_3mc$, point group: C_{6v} or $6mm$); also, a rhombohedral structure (space group: $R\cdot 3m$, point group: D_{3h} or $3m$) has been observed. The bonds in the graphene plane are strong, while the bonds between the planes are quite weak, making HOPG easy to cleave perpendicular to the *c* axis.

Optically, all the observed forms of graphite are uniaxial, where the *c* axis (and the optic axis) is perpendicular to the graphene planes. Therefore, two complex optical functions are required to describe the optical response at each wavelength: The ordinary dielectric function $\varepsilon_o(\lambda)$ describes light interaction for light polarized perpendicular to the *c* axis, while the extraordinary dielectric function $\varepsilon_e(\lambda)$ describes light interaction for light polarized along the *c* axis. The complex dielectric function $[\varepsilon(\lambda)=\varepsilon_1(\lambda)+i\varepsilon_2(\lambda)]$ is related to the complex refractive index $[\varepsilon(\lambda)=\tilde{n}^2=(n+ik)^2]$, and the optical absorption coefficient $\alpha=4\pi k/\lambda$. The quantities n and k are the refractive index and extinction coefficient, respectively, and λ is the wavelength of light.

The literature on the optical functions of graphite up to 1991 is summarized by Borghesi and Guizzetti in Ref. 4 Taft and Philipp[5] performed spectroscopic reflectivity measurements at near-normal incidence on both glassy carbon and cleaved HOPG samples, where Kramers-Kronig analysis was used to calculate $\varepsilon(\lambda)$ from the reflectivity data. Since unpolarized light was used and the angle of incidence was close to normal, the Taft and Philipp results are primarily sensitive to the ordinary optical functions $\varepsilon_o(\lambda)$. Greenaway *et al.*[6] performed polarized spectroscopic reflectivity measurements of HOPG at a variety of angles of incidence, from which they determined values of both the ordinary and extraordinary optical functions. The optical functions of graphite have also been determined using electron energy loss spectroscopy (EELS) by Venghaus.[7] Ergun[8] obtained values of ε_o and ε_e at $\lambda=546$ nm from an analysis of previous reflectance data. Polarized synchrotron measurements were also made by Klucker *et al.*[9] as a function of the angle of incidence from 3 to 40 eV. More recently, Li *et al.*[10] and Schubert[11] have examined the optical properties of HOPG in the presence of strong magnetic fields, both demonstrating Landau level splitting in the infrared. Li *et al.*[10] utilized normal-incidence reflectance measurements along the *c* axis of the graphene planes, determining the optical functions using Kramers-Kronig analysis, while Schubert[11] used terahertz spectroscopic ellipsometry.

Unfortunately, there is considerable disagreement among the various data sets. These differences may be related to a

 ©2007 The American Physical Society

number of factors, including (1) the difficulty of getting a good polished surface parallel to the c axis, (2) the difficulty of collecting all the light in a normal-incidence reflection experiment, and (3) the inherent difficulty in using Kramers-Kronig analysis to obtain optical functions from reflectivity measurements.[4] These difficulties are much more pronounced in the determination of the extraordinary optical functions, where there is conflicting evidence as to the extinction coefficient in the visible: Refs. 6 and 8 claim that the extinction coefficient is close to 0, while Ref. 7 claims that the extinction coefficient is significantly different from 0. Several theoretical investigations have been performed on the optical properties of graphite[12–16] which have been compared with the old optical data.

In this paper, we will describe an alternative technique for the determination of the optical functions of graphite in the visible part of the spectrum. This technique employs two ellipsometric measurements. First of all, we performed standard spectroscopic ellipsometry experiments on a cleaved HOPG sample at various angles of incidence. Since the c axis is close to normal to the surface, no cross polarization is expected, so the measurement can be carried out using standard ellipsometry. The second measurement is a generalized ellipsometry measurement on HOPG cut and polished such that the c axis is in the plane of the sample. While roughness is still a complicating issue with the second measurement, it perturbs the measurement considerably less at normal incidence than at the much larger angles of incidence typical of more conventional ellipsometric measurements. By combining these results of these two measurements, it is possible to obtain accurate values of n_o, k_o, n_e, and k_e at nine different wavelengths in the visible from 405 to 750 nm.

II. EXPERIMENT AND DISCUSSION

A. Sample preparation

Standard HOPG can be obtained from several sources and is generally characterized by quality. The highest quality is ZYA grade, which has a 0.4° mosaic spread of the c axis and an average grain size of 10 μm. Lower quality grades are ZYB (0.8° mosaic spread, grain size <1 μm), and ZYH (3.5° mosaic spread and grain size $\sim$40 nm). All measurements were restricted to the ZYA grade.

Two orientations of HOPG have been used to perform these measurements. The first orientation is HOPG as received where the c axis is roughly perpendicular to the sample surface ($c\perp$). This sample can be cleaned using the tape cleaving process (using a piece of adhesive tape, remove the top layer of the sample, leaving a pristine surface for measurement). The second orientation of HOPG ($c\|$) places the c axis in the plane of the sample surface, resulting in the graphene planes being perpendicular to the sample surface and roughly parallel with each other. This orientation is prepared by first encapsulating the HOPG in an epoxy matrix, which is then cut and polished to expose the edge of the HOPG. Although the $c\|$ presented surface is specular to the eye, atomic force microscopy (AFM) measurements have shown that the rms surface roughness is $\sim$5–12 nm, which is still a very rough surface for many optical measurements. As we will show below, this problem of the $c\|$ surface is minimized by performing the generalized ellipsometry measurements at near-normal incidence. An oxide layer would not be expected to form in air at room temperature on either type of surface.

B. Standard ellipsometry: c-axis normal

Although uniaxial materials may be highly optically anisotropic, there is no cross polarization for samples where the c axis is perpendicular to the sample surface. As a result, standard ellipsometry can be used to determine the pseudodielectric function of the $c\perp$ sample orientation. The pseudodielectric function is derived directly from the traditional ellipsometry parameters, and is given by

$$\langle\varepsilon\rangle = \langle\varepsilon_1\rangle + i\langle\varepsilon_2\rangle = \sin(\phi)^2\left[1 + \tan^2(\phi)\left(\frac{1-\rho}{1+\rho}\right)^2\right], \tag{1a}$$

$$\rho = \frac{r_p}{r_s} = \tan(\psi)e^{i\Delta} = \frac{C+iS}{1+N}. \tag{1b}$$

The angle of incidence is given by ϕ and ρ is the complex reflection coefficient ratio. The quantities r_p and r_s are the complex reflection coefficients for light polarized parallel and perpendicular to the plane of incidence, respectively, ψ and Δ are the traditional ellipsometric angles, and $N=\cos(2\psi)$, $S=\sin(2\psi)\sin(\Delta)$, and $C=\sin(2\psi)\cos(\Delta)$.

For isotropic samples with no surface overlayer, the pseudodielectric function becomes the actual dielectric function of the material. However, if the sample is anisotropic or has a surface overlayer, then the pseudodielectric function is perturbed somewhat from the actual dielectric function of the material. It has been shown in Ref. 17 that the pseudodielectric function for a clean (i.e., no surface overlayer) uniaxial material with the c axis normal to the surface can be expressed as

$$\langle\varepsilon\rangle \sim \frac{\varepsilon_o + \Gamma^2\sin(\phi)^2}{(1+\Gamma)^2 - \Gamma^2\sin(\phi)^2}, \tag{2a}$$

where

$$\Gamma = \frac{\varepsilon_e - \varepsilon_o}{2\varepsilon_e(\varepsilon_o - 1)} \tag{2b}$$

and ε_o and ε_e are the actual ordinary and extraordinary complex dielectric functions of the material. As can be seen from Eq. (2a), there may be a weak dependence on the angle of incidence, and the actual pseudodielectric function approaches ε_o for small values of $(\varepsilon_e - \varepsilon_o)$. However, large values of $(\varepsilon_e - \varepsilon_o)$ will result in a significant departure of $\langle\varepsilon\rangle$ from ε_o.

The ellipsometry measurements were made of the HOPG $c\perp$ sample using the two-modulator generalized ellipsometer (2-MGE)[18,19] from 220 to 860 nm (5.64–1.44 eV). Although the 2-MGE is capable of accurately measuring cross-polarization coefficients, the observed values of the cross-polarization coefficients were zero within the error limits of

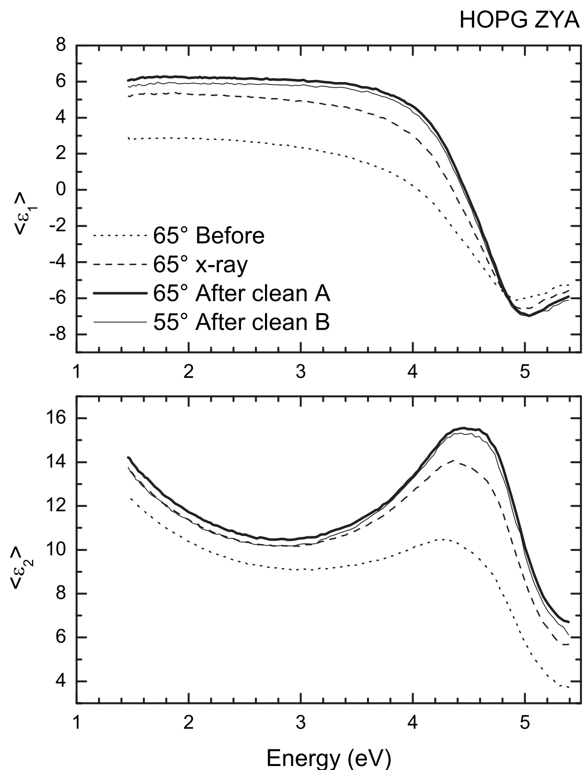

FIG. 1. Pseudodielectric functions of $c\perp$ HOPG, where the angles of incidence are listed in the figure. The before and x-ray samples were not cleaned, while the A and B samples were cleaned using the tape cleave technique described in the text.

the experiment. This is expected for uniaxial samples where the optic axis is perpendicular to the sample surface. Figure 1 shows representative pseudodielectric functions as measured on a series of HOPG ZYA quality samples with the c axis nominally perpendicular to the sample surface.

The four measurements shown in Fig. 1 are taken from different ZYA samples of HOPG. The "x-ray" sample was an old monochromator for x-ray and neutron diffraction experiments, which showed significant surface roughness. The "before" sample was a sample purchased from MikroMasch before cleaning. The two "after clean" samples were measured at different angles of incidence. The results shown are just representative; other measurements on similar samples showed similar results.

Two observations can be made:

(1) Uncleaned samples resulted in a wide variation in pseudodielectric functions where the real and imaginary parts of the pseudodielectric function are less than those of the cleaved samples (below ~4.5 eV); cleaved samples produced quite consistent values of the pseudodielectric function spectra as indicated by the cleaned spectra in Fig. 1. There was a small spread in the values of the pseudodielectric function spectra for different cleaved samples and for different spots on the same sample, probably due to variations in the sample surfaces sampled during the various measurements. The standard deviation of the various measurements resulted in an accuracy for $\langle\varepsilon_1\rangle$ and $\langle\varepsilon_2\rangle$ of ~0.05.

(2) There was a very small variation of the pseudodielectric function spectra at different angles of incidence, but this variation is less than the sample-to-sample variations mentioned above.

C. Normal-incidence generalized ellipsometry

Generalized ellipsometry was also performed on HOPG $c\|$ samples. Because of the complications resulting from the surface roughness, these measurements were performed using the two-modulator generalized ellipsometry microscope (2-MGEM), described in Refs. 18–20. Unlike the standard configuration of the 2-MGE and most other ellipsometers, the 2-MGEM is configured as a reflection microscope at near-normal incidence. Some preliminary data on similarly oriented samples of HOPG have been discussed in Refs. 21 and 22. The wavelength of operation for the 2-MGEM as presently configured was altered by changing the interference filter just after the polarization state analyzer. We have performed measurements at nine different wavelengths from 405 to 750 nm. Because many of the optical elements in the present configuration of the 2-MGEM are designed for visible operation, further significant extension of the wavelength of measurement into the UV or the IR is not possible with the present configuration. In the UV, light is cut off by the optics, while the photomultiplier tube used for these experiments is not sensitive for wavelengths greater than ~780 nm.

As discussed in Refs. 18–20, the 2-MGEM measures eight different parameters which can be related to the diattenuation N, the optical retardation δ, the direction of the principal axis γ, and the circular diattenuation CD. The signed reflection diattenuation is defined as

$$N = -\frac{R_o - R_e}{R_o + R_e}, \tag{3}$$

where R_o (R_e) is the reflectivity of the light polarized perpendicular (parallel) to the projection of the optic axis onto the surface. The reflection retardation is similarly defined as $\delta = \delta_e - \delta_o$, where δ_o and δ_e are the phase shifts for light polarized perpendicular and parallel to the c axis, respectively. As with the transmission 2-MGE,[23] the results are dual valued in that the transformation $\{N,\delta,\gamma\} \rightarrow \{-N,-\delta,\gamma+90°\}$ leaves the experimental results unchanged. The 2-MGEM is configured as a microscope where the sample is translated to acquire images of the sample and the quantities imaged are the parameters mentioned above.

Figure 2 shows a polarized light microscopy picture of the HOPG $c\|$ sample near a delamination in the material (that is, a region where the graphene planes are clearly separated by several microns) as well as a 20 μm square AFM image in the region shown in the figure. Figure 3 shows the 2-MGEM data taken near the same region as the polarized microscopy image. Both the polarized microscopy and the 2-MGEM images show that the delamination in the HOPG material is ~30 μm wide, but does not extend continuously through the material. Moreover, there are also smaller delaminations that are ~30–300 μm long and <10 μm wide. The polarized light microscope image shows varying contrast due to slight changes in the polarization-dependent reflective properties of the material, while the 2-MGEM measurement quantifies this

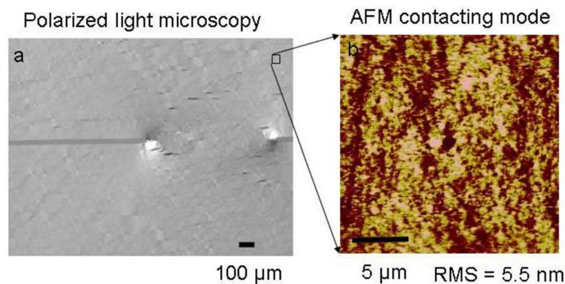

FIG. 2. (Color online) Polarized microscope picture of HOPG (a) and an AFM contacting mode image of the $20 \times 20\ \mu m^2$ region indicated (b). The rms roughness from the AFM image was 5.5 nm and the z-height scale was 0–20 nm.

observation. Near the ends of the main 30 μm wide delamination, the polarized light microscope picture shows a bright spot above (below) one end point, and below (above) at the other end point. The 2-MGEM images show why: the direction of the principal axis (that is, the directions of the graphene planes) changes considerably in these regions, while the diattenuation N and the retardation δ do not. If we look at one of the other regions of delamination (shown by the expanded scale plots to the left of Fig. 3), we see that there is very little change in N and δ just outside the fissure, but there is a significant change is the direction of the principal axis γ.

In regions where there are no delaminations, there are much smaller variations in the polarization optical properties. Between the two ends of the major delamination in Fig. 3, there is a small decrease in N and $|\delta|$ in an arc above and below the connecting line. This decrease is real in that it is greater than the errors of the individual measurements. In other regions (such as the upper-right hand part of the central plots of Fig. 3), the values of N, δ, and γ are relatively uniform.

To obtain accurate values of N and δ for HOPG, we performed a series of 2-MGEM measurements near the uniform area shown in the upper-right hand corner of Fig. 3 and near the box indicated in Fig. 2 where the AFM measurements were made. The sample area consisted of a rectangle 410 $\times 390\ \mu m^2$, sampled at 10 μm intervals (1599 total points). Measurements were taken at nine different wavelengths between 405 and 750 nm. The resulting values of N and δ are shown in Fig. 4 along with the standard deviations resulting from averaging over 1599 points.

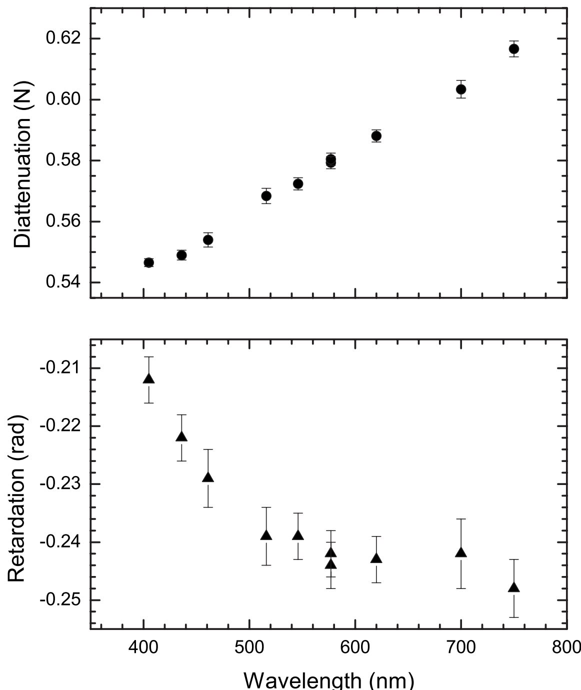

FIG. 4. Diattenuation N and retardation δ for HOPG $c\|$ averaged over 1599 points. The error limits show the standard deviation of the measurements.

III. ANALYSIS AND RESULTS

The two measurements discussed above each produce two measured values, so it may be possible to determine the complex dielectric functions or complex refractive indices (also four values) at the nine measured wavelengths. This assumes that we can correct appropriately for any surface roughness

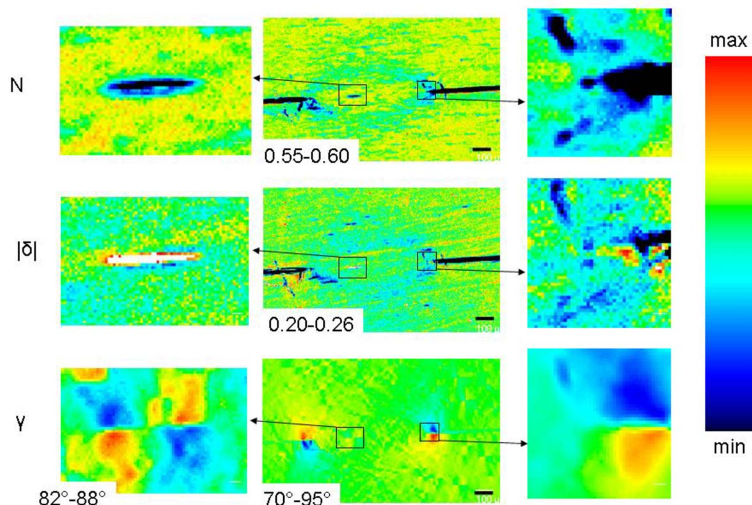

FIG. 3. (Color online) 2-MGEM data for the same sample shown in Fig. 2. The images show the diattenuation N, the absolute retardation $|\delta|$, and the direction of the fast axis γ. The pictures to the left and right show two selected regions at higher magnification. The black mark in the lower right corner of the center images indicates 100 μm. The color scale for the maximum and minimum values is shown to the right. The optical resolution is 4 μm and the pixel size is 2.5 μm.

of the samples and that there are no significant correlations. The pseudodielectric function increases to a relatively constant value after the tape cleaving process (see Sec. II B), so we can assume that there is no significant surface roughness remaining after this process. However, the samples oriented such that the c axis is parallel to the sample surface obviously have significant surface roughness as measured by AFM, which must be taken into account.

If a 2-MGEM measurement is made at normal incidence on a uniaxial sample, oriented with the c axis in the plane of the sample and without surface roughness, then the N, S, and C parameters are given by[20]

$$N = 2\frac{\mathrm{Re}(r_d)}{r_d r_d^* + 1}, \tag{4a}$$

$$S = 2\frac{\mathrm{Im}(r_d)}{r_d r_d^* + 1}, \tag{4b}$$

$$C = \frac{r_d r_d^* - 1}{r_d r_d^* + 1}. \tag{4c}$$

The complex reflection ratio r_d is given by

$$r_d = \frac{r_o - r_e}{r_o + r_e}, \tag{4d}$$

$$r_o = \frac{\tilde{n}_o - 1}{\tilde{n}_o + 1}, \tag{4e}$$

$$r_e = \frac{\tilde{n}_e - 1}{\tilde{n}_e + 1}, \tag{4f}$$

and the parameters $\tilde{n}_o$ and $\tilde{n}_e$ are the complex ordinary and extraordinary refractive indices, respectively. Clearly, N, S, and C are not independent, since $N^2+S^2+C^2=1$.

The effects of surface roughness can be included into r_o and r_e using the standard Airy formula

$$r = \frac{r_{af} + r_{fs}e^{2i\beta}}{1 + r_{af}r_{fs}e^{2i\beta}}, \tag{5}$$

where $\beta = 2\pi d_f \tilde{n}_f/\lambda$, d_f being the roughness film thickness, $\tilde{n}_f$ the roughness film complex refractive index, and λ being the wavelength of light. The complex reflection coefficients are given by $r_{af} = (\tilde{n}_f - 1)/(\tilde{n}_f + 1)$ and $r_{fs} = (\tilde{n}_s - \tilde{n}_f)/(\tilde{n}_s + \tilde{n}_f)$ where $\tilde{n}_s$ is the complex refractive index of the substrate. The roughness refractive index $\tilde{n}_f$ is approximated using the Bruggeman effective medium approximation,[24] calculated using the technique of Roussel *et al.*[25]

For a given value of the surface roughness, it is possible to determine the ordinary and extraordinary values of the complex dielectric function from the data presented in Figs. 1 and 4 using the expressions in Eqs. (2), (4), and (5). To prevent possible false solutions, a grid search approach was used with an initial solution search from 1 to 8 for n_o and n_e and from 0 to 5 for k_o and k_e, where the goodness-of-fit parameter was the reduced χ^2,

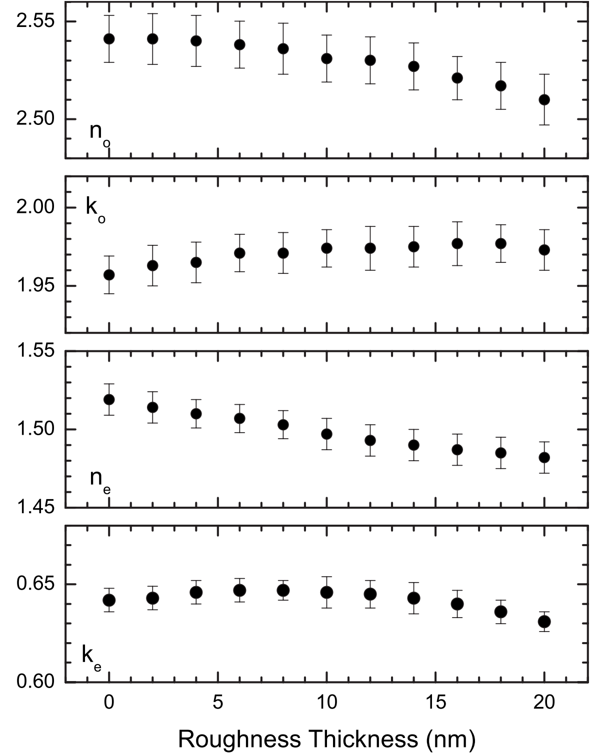

FIG. 5. The calculated values of the complex refractive index for light polarized perpendicular to the optic axis (ordinary, n_o, k_o) and for light polarized parallel to the optic axis (extraordinary, n_e, k_e) as a function of the thickness of the surface roughness. The wavelength was 577 nm.

$$\chi^2 = \frac{1}{4}\left(\frac{(\langle\varepsilon_{1,\mathrm{expt}}\rangle - \langle\varepsilon_{1,\mathrm{calc}}\rangle)^2}{\delta\varepsilon_1^2} + \frac{(\langle\varepsilon_{2,\mathrm{expt}}\rangle - \langle\varepsilon_{2,\mathrm{calc}}\rangle)^2}{\delta\varepsilon_2^2} + \frac{(N_{\mathrm{expt}} - N_{\mathrm{calc}})^2}{\delta N^2} + \frac{(S_{\mathrm{expt}} - S_{\mathrm{calc}})^2}{\delta S^2}\right). \tag{6}$$

Solutions were refined using a sequential Monte Carlo search, resulting in final values of $\chi^2 < 0.06$, indicating that a good fit was obtained. Correlated errors of n_o, k_o, n_e, and k_e were determined by finding the axes of the hyperellipsoid defined by $\chi^2 < 1$; all correlated errors were < 0.015, indicating that there is no significant correlation. This procedure was performed for 11 different values of surface roughness (0–20 nm in steps of 2 nm), and the results for the $\lambda = 577$ nm data are shown in Fig. 5.

Compared to the errors of the individual data points, there is a small effect of surface roughness on the value of n_e, but not on the final values of n_o, k_o, and k_e. Therefore, we select the values calculated for 10 nm surface roughness and appropriately adjust the final error to take into account the uncertainty in the surface roughness. The values of the complex dielectric functions determined from this work are listed in Table I for the complex refractive index and the resulting complex dielectric functions are shown in Fig. 6.

IV. DISCUSSION

It is instructive to compare these results with other results in the literature (shown in Table II). For this comparison, we

TABLE I. Complex refractive indices and calculated polarized reflectivities for HOPG at different wavelengths.

Wavelength (nm)	n_o	k_o	n_e	k_e	R_o	R_e
405	2.51	1.88	1.53	0.66	0.367	0.105
436	2.52	1.87	1.52	0.66	0.0366	0.104
461	2.51	1.88	1.51	0.66	0.0367	0.103
516	2.51	1.92	1.50	0.65	0.372	0.101
546	2.52	1.94	1.50	0.65	0.376	0.101
577	2.53	1.97	1.50	0.65	0.381	0.100
620	2.55	2.02	1.50	0.64	0.388	0.100
700	2.58	2.10	1.50	0.63	0.401	0.098
750	2.59	2.16	1.49	0.63	0.410	0.096
Ave. error	0.01	0.02	0.02	0.01	0.002	0.001

have chosen the data at 546 nm. Much of the available data concludes that the ordinary extinction coefficient is significantly different from 0, although there are significant differences in the actual values. Furthermore, there is considerable variance between the obtained values of the refractive index for the ordinary polarization. The probable problem with these data sets is that they were obtained using reflectivity measurements, possibly followed with Kramers-Kronig analysis. As can be seen from the values of the reflectivity, measured and calculated, the values are considerably lower than the reflectivity calculated from this work. Thus, one can conclude that the previous measurements probably did not collect all the reflected light from the rough HOPG samples; this possible difficulty was stated by Borghesi and Guizzetti.[4]

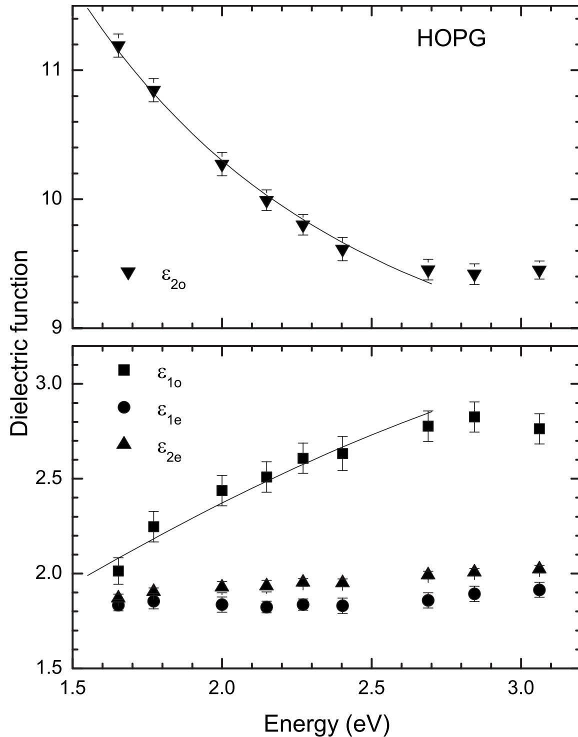

FIG. 6. The real and imaginary parts of the complex dielectric function for light polarized perpendicular (o) and parallel (e) to the optic axis. The line shows the best fit obtained using the Drude-like expression in Eqs. (7) (see text).

It is even more difficult to obtain good values of the optical functions for the extraordinary light polarization. Greenaway *et al.*[6] claimed that $k_e=0$, while Ergun[8] was not able to obtain a value. Venghaus[7] obtained values of n_e and k_e using EELS. Using these published values for the complex refractive indices, we can calculate the values of N, S, and C expected for the normal-incidence 2-MGEM measurement using Eqs. (4) above (see Table II). Clearly, the values of N, S, and C calculated from the complex refractive index data of the earlier work do not agree with the present results. The implications are significant: If $k_e=0$, then no direct optical transitions are allowed at this wavelength nor can there be significant numbers of free carriers. If $k_e>0$, then either direct optical transitions are allowed and/or free carriers are excited that can be probed with light polarized perpendicular to the graphene plane.

The main difference between this work and the previous determinations of the optical functions of graphite is that this work uses ellipsometric techniques, while the previous work used reflectance techniques. One of the primary advantages of the ellipsometric technique is that it is not necessary to collect all the light, since ellipsometry is inherently a ratio method; light scattered out of the collection cone of the optics does not contribute to the measurement thereby not biasing the final result. With very rough samples such as HOPG, this is critical.

One potential criticism to the determination of the optical functions shown in this work concerns the incorporation of the surface roughness. Indeed, the significant variation of the diattenuation and retardation due to imperfections of the $c\|$ surface (see Figs. 2 and 3) show that certain regions must be avoided to improve the accuracy of the measurement. This is done here by selecting a region where there are no obvious features in N, δ, or γ. Surface roughness features on a subwavelength scale, as shown by the AFM measurements [see Fig. 2(b)], are also a potential cause of errors in the final values of the complex dielectric function. However, Fig. 4 shows that the values of the complex refractive indices are not significantly changed by the addition of a small surface roughness. This might be expected since it is well known that normal-incidence reflectivity is not significantly affected by films much less than the wavelength of light.

As can be seen from Fig. 6, the complex dielectric functions for graphite are quite different for light polarized parallel to the optic axis (extraordinary) compared to light polarized perpendicular to the optic axis (ordinary). The ordinary component shows the classic behavior of quasi-free-carrier behavior in that the imaginary part (ε_{2o}) increases with decreasing energy, while the real part (ε_{1o}) decreases with decreasing energy. The data in Fig. 6 for $\lambda>460$ nm (<2.7 eV) were fitted to the Drude-like form

$$\varepsilon_{1\mathrm{D}} = \varepsilon_{1o} - \frac{E_p^2\tau^2}{1+E^2\tau^2},$$

TABLE II. Comparison of the various optical functions at 546 nm (=2.27 eV). The values of the reflectivity, N, S, and C are either calculated from the values of the appropriate n and k or taken from figures in the appropriate references. The values of n and k from Taft and Philipp (Ref. 5) and from Greenaway *et al.* (Ref. 6) are taken from the figures of Ref. 6, which may influence the error of these values. Similarly, the values of n and k for Venghaus (Ref. 7) are taken from the table in Ref. 4. The values of n and k for Li *et al.* (Ref. 10) are determined from the experimental reflectance and optical conductivity determined by Kramers-Kronig analysis at 0 magnetic field (Figs. 1 and 4 from Ref. 10).

	n_o	k_o	n_e	k_e	R_o	R_e	N	S	C
This work	2.52	1.94	1.50	0.65	0.376[a]	0.101[a]	0.572[b]	−0.195[b]	−0.796[b]
T&P[c]	2.57[b]	1.41[d]			0.302[a] 0.297[b]				
Greenaway *et al.*[e]	2.70[d]	1.35[d]	1.55[d]	0.00[d]	0.306[a] 0.346[b]	0.047[a]	0.367[a]	0.107[a]	−0.644[a]
Ergun[f]	2.15	0.66	1.81		0.170[a]	0.083[a]	0.171[a]	0.145[a]	−0.893[a]
Venghaus[g]			2.02[h]	0.68[h]		0.157[a]			
Li *et al.*[i]	3.64	0.44			0.33[b]				

[a]Calculated from the values of n and k given in the table.
[b]Measured values taken from the Reference.
[c]Reference 5.
[d]Taken from Figs. 5 and 6 of Ref. 6.
[e]Reference 6.
[f]Reference 8.
[g]Reference 7.
[h]Interpolated from the table in Ref. 4.
[i]Reference 10.

$$\varepsilon_{2D} = \varepsilon_{2o} + \frac{\tau}{E} \frac{E_p^2}{(1 + E^2\tau^2)}, \tag{7}$$

where ε_{1o} and ε_{2o} are contributions that are not related to free carriers, E_p is the plasma energy, and the τ is related to the mean time between collisions $t_c = h\tau/2\pi$. From the fits, it was determined that $\varepsilon_{1o}=4.21$, $\varepsilon_{2o}=8.19$, $E_p=4.13$ eV, and $t_c=2.86\times10^{-16}$ s. The fit was limited to the visible and IR regions of the spectrum to avoid the effects of the plasmon peak near 4.5 eV (see Fig. 1). Note that the Drude-like fit of Eq. (7) is equivalent to a Lorentzian fit where the resonant energy is 0; a Lorentzian fit with a very small resonant energy (such as discussed in Refs. 10 and 11) would give equivalent results in this wavelength region.

Clearly, it is not possible to fit the data in Fig. 6 using a strictly Drude-like free-carrier dielectric function (where $\varepsilon_{1o}=1$ and $\varepsilon_{2o}=0$), indicating that there is some significant band-to-band absorption also taking place in this energy region. Data extending more into the IR would obviously be beneficial here.

The extraordinary complex dielectric function behaves in a decidedly different way (see Fig. 6). Not only are the values considerably different from the values of the ordinary complex dielectric functions, but there is no obvious Drude-like behavior as the photon energy decreases. Also, the value of ε_{2e} is significantly different from 0, showing that graphite cannot be an insulator in the visible part of the spectrum. Therefore, HOPG behaves like a low carrier-density metal, semimetal, or semiconductor for visible light polarized perpendicular to the graphene plane. This is consistent with the two-dimensional Landau quantization observed in the terahertz region discussed in Ref. 11

V. CONCLUSIONS

In this work, we have obtained the ordinary and extraordinary optical functions of highly oriented pyrolytic graphite (HOPG). These values were obtained using standard ellipsometry measurements on cleaned HOPG samples where the c axis was perpendicular to the sample surface, and near-normal incidence generalized ellipsometry on samples cut such that the c axis was in the plane of the sample. The results from these measurements are compared with previous determinations of the optical functions, from which it can be concluded that nonspecular reflections from HOPG in the older work contributed errors to the interpretation of the results.

The ordinary dielectric functions (for light polarized perpendicular to the optic axis) show Drude-like free-carrier optical response in addition to band-to-band transitions; this agrees with the results of Ref. 10 in the visible part of the spectrum. The extraordinary dielectric functions (for light polarized parallel to the optic axis) show nearly constant values of $\varepsilon_{1e}(\lambda)$ and $\varepsilon_{2e}(\lambda)$ from $\lambda=405$ to 750 nm (and thus no obvious effects from free-carrier absorption); over this wavelength range, $\varepsilon_{2e}(\lambda)$ is clearly greater than 0, contrary to other results in the literature (see Refs. 6 and 8). Therefore, HOPG behaves as a traditional metal for visible light polarized parallel to the graphene planes, but as a semiconductor or semimetal for visible light polarized perpendicular to the graphene planes.

The two-modulator generalized microscope (2-MGEM) was used to generate images of the diattenuation and optical retardation for cross sections of HOPG. While polarized light micrographs show features in the images, the 2-MGEM images show why distortions of the graphene planes near some defects result in local changes in the optical properties, particularly in the local direction of the *c* axis. While the direction of the optic axis of HOPG is nearly constant over most of the sample, it can change by several degrees near large defects (such as delaminations in the HOPG). These areas have been avoided in the determination of the optical properties presented in this paper.

ACKNOWLEDGMENTS

Research sponsored by the DOE Office of Basic Energy Sciences, Division of Materials Sciences and Engineering and the DOE Office of Nuclear Energy, Science and Technology's Advanced Gas Reactor program. Research performed at the Oak Ridge National Laboratory, managed and operated by UT-Battelle, LLC.

[1] M. S. Dresselhaus and M. Endo, Top. Appl. Phys. **80**, 11 (2001).
[2] A. W. Moore, A. R. Ubbelohde, and D. A. Young, Proc. R. Soc. London, Ser. A **280**, 153 (1964).
[3] R. W. G. Wyckoff, *Crystal Structures* (Wiley, New York, 1963), Vol. 1.
[4] A. Borghesi and G. Guizzetti, *Handbook of Optical Constants of Solids II*, edited by E. D. Palik (Academic, New York, 1991).
[5] E. A. Taft and H. R. Philipp, Phys. Rev. **138**, A197 (1965).
[6] D. L. Greenaway, G. Harbeke, F. Bassani, and E. Tosatti, Phys. Rev. **178**, 1340 (1969).
[7] H. Venghaus, Phys. Status Solidi B **71**, 609 (1975).
[8] S. Ergun, Nature (London) **213**, 135 (1967).
[9] R. Klucker, M. Skibowski, and W. Steinmann, Phys. Status Solidi B **65**, 703 (1974).
[10] Z. Q. Li, S.-W. Tsai, W. J. Padilla, S. V. Dordevic, K. S. Burch, Y. J. Wang, and D. N. Basov, Phys. Rev. B **74**, 195404 (2006).
[11] M. Schubert, Ann. Phys. **15**, 480 (2006).
[12] G. S. Painter and D. E. Ellis, Phys. Rev. B **1**, 4747 (1970).
[13] L. G. Johnson and G. Dresselhaus, Phys. Rev. B **7**, 2275 (1973).
[14] R. Ahuja, S. Auluck, J. M. Wills, M. Alouani, B. Johansson, and O. Eriksson, Phys. Rev. B **55**, 4999 (1997).
[15] A. B. Djurisic and E. H. Li, J. Appl. Phys. **85**, 7404 (1999).
[16] T. G. Pedersen, Phys. Rev. B **67**, 113106 (2003).
[17] G. E. Jellison, Jr. and J. S. Baba, J. Opt. Soc. Am. A **23**, 468 (2006).
[18] G. E. Jellison, Jr. and F. A. Modine, Appl. Opt. **36**, 8184 (1997).
[19] G. E. Jellison, Jr. and F. A. Modine, Appl. Opt. **36**, 8190 (1997).
[20] G. E. Jellison, Jr., J. D. Hunn, and C. M. Rouleau, Appl. Opt. **45**, 5479 (2006).
[21] G. E. Jellison, Jr., D. E. Holcomb, J. D. Hunn, C. M. Rouleau, and G. W. Wright, Appl. Surf. Sci. **253**, 47 (2006).
[22] G. E. Jellison, Jr., J. D. Hunn, and R. A. Lowden, J. Nucl. Mater. **352**, 6 (2006).
[23] G. E. Jellison, Jr., C. O. Griffiths, D. E. Holcomb, and C. M. Rouleau, Appl. Opt. **41**, 6555 (2002).
[24] D. A. G. Bruggeman, Ann. Phys. **24**, 636 (1935).
[25] Ph. J. Roussel, J. Vanhellemont, and H. E. Maes, Thin Solid Films **234**, 423 (1993).